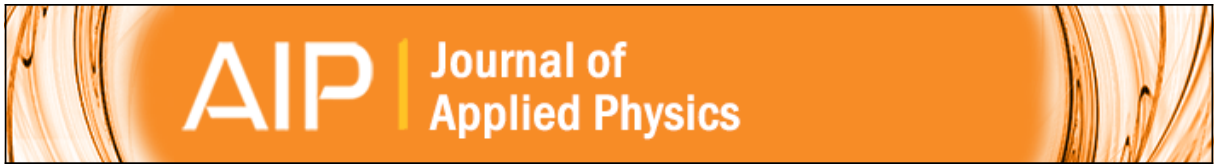

Extracting composition and alloying information of coherent Ge(Si)/Si(001) islands from [001] on-zone bright-field diffraction contrast images

X. Z. Liao, J. Zou, D. J. H. Cockayne, Z. M. Jiang, and X. Wang

Citation: Journal of Applied Physics **90**, 2725 (2001); doi: 10.1063/1.1394900

View online: http://dx.doi.org/10.1063/1.1394900

View Table of Contents: http://scitation.aip.org/content/aip/journal/jap/90/6?ver=pdfcov

Published by the AIP Publishing

Extracting composition and alloying information of coherent Ge(Si)/Si(001) islands from [001] on-zone bright-field diffraction contrast images

X. Z. Liao[a] and J. Zou
Australian Key Centre for Microscopy and Microanalysis, The University of Sydney, Sydney NSW 2006, Australia

D. J. H. Cockayne
Department of Materials, University of Oxford, Parks Road, Oxford OX1 3PH, England

Z. M. Jiang and X. Wang
Surface Physics Laboratory, Fudan University, Shanghai 200433, People's Republic of China

(Received 5 March 2001; accepted for publication 24 June 2001)

Ge(Si)/Si(001) coherent islands grown at 700 °C by molecular beam epitaxy were investigated using transmission electron microscopy. [001] on-zone bright-field diffraction contrast imaging and image simulation techniques were used to investigate the structure of these coherent islands. Comparison of simulated and experimental images indicates nonuniform composition distribution within the coherent islands when the islands were grown at high temperatures (700 °C), but uniform composition for growth at lower temperatures (600 °C). © *2001 American Institute of Physics.* [DOI: 10.1063/1.1394900]

INTRODUCTION

Semiconductor quantum dots (QDs) have important potential applications in optoelectronic devices[1] and quantum computers.[2] Knowledge of the structural parameters of QDs including the shape, size, and composition at different stages of QD island growth is important for revealing information on the QD growth mechanism and for understanding the structure-property relationship of the QDs.[3] Although many techniques can be used to investigate the QD shape and size, only a few techniques are available for the determination of local composition. These include scanning tunneling microscopy,[4] high-resolution x-ray diffraction analysis,[5] and some transmission electron microscopy (TEM) techniques including high-resolution imaging combined with finite element analysis,[6] electron energy loss spectrometry,[7] and x-ray energy dispersive spectrometry (EDS).[8,9] For each of the above TEM studies, very thin cross-section TEM specimens are required. However, it is difficult to prepare cross-section TEM specimens, especially for samples with low QD densities, and even then the section might include any part of the QD. As a result, there is an advantage in using plan-view specimens, as have been used for investigating planar distributions and for estimating QD lateral sizes.

It is well known that, under dynamical two-beam or on-zone axis multibeam TEM imaging conditions, diffraction contrast of lattice mismatch coherent QDs arises largely from the strain field around and within the QDs,[10,11] rather than from the QD shape and size directly. This makes it complicated to correlate the shape and size of QD islands and their TEM images.[10] However, because the QD strain field is sensitive to its composition, it is possible to extract composition information about QDs from the diffraction contrast images through image simulations.[12] In our earlier study of InGaAs/GaAs system,[12] it was shown that TEM images taken under on-zone axis conditions contain image detail which is sensitive to the QD composition. In this study, we deduce the composition in Ge(Si)/Si(001) coherent islands from plan-view TEM using the same simulation technique, which involves finite element analysis to generate the strain field and the dynamical diffraction theory to simulate the images.

EXPERIMENTS

p-type Si(001) wafers with resistivity of 1 Ω cm were used as a substrate. Ge islands were grown on the Si substrates by solid source molecular beam epitaxy (MBE) with a deposition thickness of 0.8 nm at a growth temperature of 700 °C and a growth rate of 0.02 nm/s. Prior to Ge deposition, a 30-nm-thick Si buffer layer was grown on the substrate. Ge island growth at this high temperature results in a strong alloying effect through the diffusion of substrate material Si into the Ge islands to reduce the misfit strain energy.[13]

Plan-view TEM specimens were prepared using chemical etching with a solution of HF and HNO_3 in the ratio of 1:9. Cross-section TEM specimens were prepared using Ar+ ion-beam thinning in a Gatan precision ion polishing system with an accelerating energy of 3 keV. Cross-section TEM investigations were carried out using a Philips CM12 operating at 120 keV, and plan-view TEM observations were carried out using a Philips EM430 operating at 300 keV.

Figure 1(a) is an experimental plan-view [001] on-zone bright-field diffraction contrast image, showing randomly distributed coherent islands. The islands are uniform in size and have approximately square-shaped image boundaries with rounded corners. Figure 1(b) shows two other islands at a higher magnification to give details of the image feature

[a]Present address: Division of Materials Science and Technology, Los Alamos National Laboratory, Los Alamos, NM 87545. Electronic mail: xzliao@lanl.gov

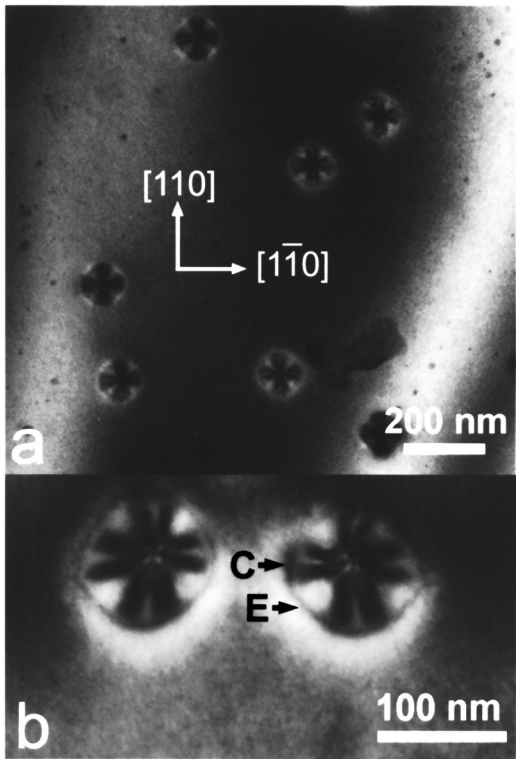

FIG. 1. Plan-view [001] on-zone bright-field diffraction contrast images (a) showing random distribution of coherent Ge(Si) islands and (b) showing detailed image features at a larger magnification; (a) and (b) are taken from different areas.

which are: (i) each coherent island is surrounded by a dark square line with rounded corners and the square line is thicker at the island corners [see the area marked with "*C*" in Fig. 1(b)] and thinner at the island edges [see the area marked with "*E*" in Fig. 1(b)] and (ii) inside the dark square line of each island is a double-cross with the bars of the double-cross approximately parallel to ⟨110⟩ with the distances between the coupled bars of the double cross wider at the island corners.

As was emphasized in Ref. 12, the diffraction contrast arises largely from the strain field within and around the coherent islands, and the strain field is a function of the island shape, size, and composition. Therefore, to extract composition information from the diffraction contrast images in Fig. 1 through image simulations, knowing the shape and

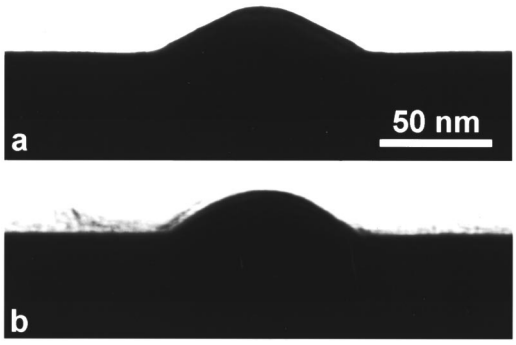

FIG. 2. Cross-section images of a coherent Ge(Si) island viewed along (a) ⟨110⟩ and (b) ⟨100⟩.

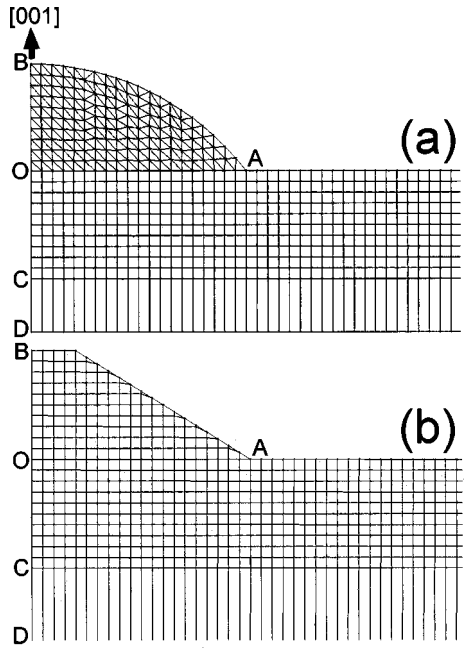

FIG. 3. Models of the (100) cross section of (a) a spherical-cap-shaped island and (b) a truncated pyramidal shaped island. Only half of the models are shown as they are symmetrical about the axis [001] (OB). The dimension of CD is adjustable depending on the thickness of the substrate.

size of the coherent island is essential. To determine these structural parameters, cross-section TEM specimens were obtained. Figures 2(a) and 2(b) show typical examples of side projection images of a coherent island taken along ⟨110⟩ and ⟨100⟩, respectively. The images were taken from an area with a very thick substrate so that the island profile was protected by the thick substrate from any damage caused by ion-beam thinning during specimen preparation. In our earlier work,[13] trenches around islands were found. Such trenches would not be visible in these images because it would be masked by the thick substrate. It is seen that the island has a trapezoid-shaped ⟨110⟩ side projection and a lens-shaped ⟨100⟩ side projection. These projected shapes agree with those reported by Chaparro *et al.*[14] using atomic force microscopy. Figure 2(a) shows the island having a base diameter of approximately 100 nm and a height-to-base diameter ratio of about 1:4.6, while Fig. 2(b) shows the island base edge length of about 90 nm and an aspect ratio of 1:4.2. In general, the aspect ratios of the islands in this investigation are between 1:4 and 1:5.

IMAGE SIMULATIONS

From Fig. 2, it is clear that the shape of the coherent Ge(Si)/Si island is complicated and can be regarded as a combination of a lens shape and a truncated pyramidal shape. To simplify the mathematical models of the island shape for the purposes of strain field calculations and image simulations, both the lens shape and the truncated pyramidal shape, which are the two extreme of possible island shapes, are used in this investigation. The strain field calculations were carried out by finite element analysis using STRAND6 software.[15]

Figure 3 shows the two finite element models in cross section along ⟨100⟩. For the lens-shaped model, a spherical-cap-shaped island is employed for simplicity. The fine lines in the two models are the finite element meshes used in the calculation. In the two models, the half width of the coherent island (OA) has been set at 50 nm and equal to $4R/5$ for the case of the spherical-cap shape (R is the radius of the sphere) and the height (OB) has been set to 25 nm and equal to $2R/5$, so that the height-to-base diameter (in the case of spherical-cap shape) and the height-to-edge length (in the case of truncated pyramidal shape) ratios are 1:4 to match the experimental data.

For the spherical-cap shape, three-dimensional models were generated by rotating the two-dimensional section in Fig. 3(a) by 90° around [001]. The geometry is meshed with eight-node hexahedron elements in most of the substrate area, six-node wedge elements in the substrate area connecting the rotation axis COB, six-node wedge elements in most of the island, and with four-node tetrahedron elements in the island area connected with COB. Because (i) the model has axial symmetry around [001] and (ii) the crystal lattice of the sample has fourfold symmetry, only one-quarter of the model needs to be calculated. Boundary conditions are set by the fourfold symmetry of the strain field and by assuming that QDs are periodically arrayed in [100] and [010] directions.

For the truncated pyramidal shape in Fig. 3(b), three-dimensional models were generated by building the three-dimensional elements in the coherent island one-by-one. In the substrate area, large elements were generated first and then were subdivided into smaller elements. A combination of eight-node hexahedron elements, six-node wedge elements, and four-node tetrahedron elements were used in the finite element models. The truncated pyramid has edges parallel to ⟨100⟩ and ridges on island surface in the (110) and (1-10) planes passing through COB. Because the geometric model and the crystal lattice have a fourfold symmetry, only one-quarter of the model was calculated. Boundary conditions are set the same as in the case of the spherical-cap in Fig. 3(a).

In the two models, the lattice mismatch (f) between the island and the substrate is introduced by putting the thermal expansion coefficients as f (K^{-1}) for the island and 0 (K^{-1}) for the substrate, and then by raising the temperature by 1 K.

Following the procedures of Ref. 12, image simulations were carried out using multibeam dynamical electron scattering theory[16] with the column approximation. Absorption was included using the perturbation method assuming the imaginary parts of Fourier coefficients of lattice potential to be one-tenth of their real counterparts.[16] Calculations with different absorption coefficient values showed no significant differences to the images, except changes in relative contrast. During the image simulations, column approximation calculations were performed for the square simulation area (with square edges parallel to ⟨100⟩) of $2d \times 2d$ (where d is the base diameter or base edge length of the model coherent islands) which was divided into 80×80 columns, so that each column has a diameter of 2.5 nm. Other parameters used in the simulations are: sample thickness (measured from the substrate bottom to the top of the coherent islands), 80 nm;[17] electron accelerating voltage, 300 kV; and number of electron beams included in the image simulations, 21. Note that the number of the electron beams included in the image simulations must be $4n+1$, where $n=1,2,3,...$, to ensure the fourfold symmetry of the diffraction pattern under the [001] zone-axis diffraction condition. Test simulations show that the image features remain unchanged for simulations with $n \geqslant 9$.

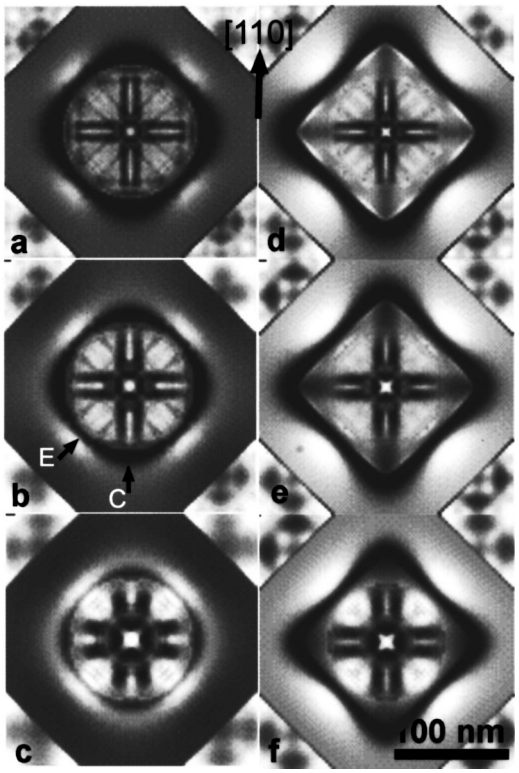

FIG. 4. Simulated images for model spherical cap [(a)–(c)] and truncated pyramid [(d)–(f)] islands with a base diameter/edge length 100 nm, an aspect ratio of height-to-base diameter/edge length 1:4, and lattice mismatches (a) and (d) 4%, (b) and (e) 3%, and (c) and (f) 2%.

Figure 4 shows simulated images for the two island models with a base diameter/edge length of 100 nm and an aspect ratio of height-to-base diameter (or height-to-base edge for truncated pyramid) of 1:4. Figures 4(a)–4(c) are simulated images for the spherical-cap shaped model with different lattice mismatches of 4% (almost pure Ge in the model island), 3% and 2%, respectively. Figures 4(d)–4(f) are simulated images for the truncated pyramidal shaped model also with different lattice mismatches of 4%, 3%, and 2%, respectively. As expected, the shapes of image boundaries for the two models are different. However, the following features in the simulated images are independent of the island shape: (i) each island is surrounded by a dark square line that appears thicker at corners along ⟨110⟩ [see Fig. 4(c) an arrow marked with "*C*"] and thinner at edges along ⟨100⟩ [see Fig. 4(c) an arrow marked with "*E*"]; (ii) the images show a distinct double cross with parallel bars along ⟨110⟩; and (iii) the distance between the coupled parallel bars increases as the lattice mismatch is reduced.

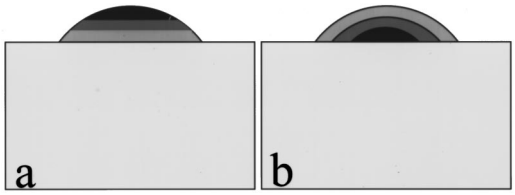

FIG. 5. Schematic diagrams showing model spherical-cap coherent islands with composition gradients for (a) a layer structure and (b) a shell structure. The compositions are represented by the gray scale with darker area has higher Ge content.

Comparing Figs. 4 and 1, it is seen that the main features referred to above occur both in the simulated and the experimental images, except that the coupled bars in the simulated images are parallel while the coupled bars in the experimental images diverge from the island center. In a previous study,[12] a similar feature of images from InGaAs/GaAs QD islands was explained as being due to a segregation of elements within the islands. Composition gradients in Ge(Si) coherent islands have also been reported by high-resolution x-ray diffraction analysis[5] and high-spatial-resolution EDS measurements.[9] For this reason, image simulations for model coherent islands with a composition gradient along a vertical direction were carried out. This was done by varying the lattice mismatch in different layers of model islands. A schematic diagram for the case of the spherical-cap model is shown in Fig. 5(a). Figure 6(a) shows a simulated image of a spherical-cap model with the lattice mismatches in the island varying from 0.25% at the island bottom to 3% at the island top. Figure 6(b) shows a simulated image of a truncated pyramid model with the lattice mismatches in the island varying from 1.5% at the island bottom to 3% at the island top.[18] It is seen, in Fig. 6, that for both cases the coupled bars are no longer parallel, but widen at the island corners. These images are in excellent agreement with the experimental image [as shown in Fig. 1(b)], suggesting that composition segregation exists in the studied coherent islands.

Several other composition segregation models have also been tested. One of these, in which the model is of a shell structure with the largest Ge content in the island core and the lowest Ge content at the outmost shell [see Fig. 5(b)], has image features similar to those shown in the experimental images. Other models, for example, cylinder structures, a shell structure with the largest Ge content at the outermost shell, and a layer structure with the largest Ge content at the bottom layer, do not present images of double crosses with diverged coupled bars.

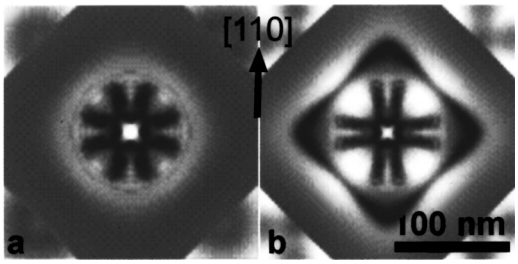

FIG. 6. Simulated images for (a) model spherical cap with the lattice mismatch varying from 0.25% at the island bottom to 3% at the island top and (b) model truncated pyramid with lattice mismatch varying from 1.5% at the island bottom to 3% at the island top.

DISCUSSION

Although the above image simulations cannot differentiate between the segregation models in Fig. 5, it is noted that, for high temperature growth of Ge(Si) islands, element mobility is high and the system is likely to adopt a structure which is energetically favorable. This would favor the model in Fig. 5(a) over the model in Fig. 5(b), because Fig. 5(b), with the larger element Ge in the island center, has a high strain energy. This argument is indirectly supported by the fact that dislocated Ge(Si)/Si(001) islands grown at the same temperature of 700 °C have a composition distribution similar to the model of Fig. 5(a).[8]

In addition, composition nonuniformity of coherent islands has also been reported in an alloy system of $Si_{0.75}Ge_{0.25}Si(001)$ grown by liquid phase epitaxy. Wiebach *et al.*[5] investigated the composition of coherent $Si_{0.75}Ge_{0.25}Si(001)$ islands using x-ray scattering. In order to simplify their calculation, they assumed a vertical composition profile and found that a composition gradient model with more Ge content at the top part of the islands gave a better agreement between experimental and calculated data.

It is interesting to note that double-cross contrast has been reported previously by Wöhl *et al.*,[19] and Sakamoto *et al.*[20] for Ge/Si(001) islands grown by MBE at different temperatures. For the sample grown at 720 °C,[19] similar nonparallel coupled bars are seen, while for the samples grown at 600 °C,[20] the coupled bars are parallel to each other and the distance between the coupled bars is narrower (from Fig. 4, such narrower coupled bars imply a higher Ge composition). These results suggest that a higher growth temperature results in a larger alloying effect and that the element segregation within the coherent islands is a common phenomenon for high temperature growth of Ge/Si islands.

Uniformity in the shape and size of QD islands is required in many applications. Investigations have showed that QD growth at high temperatures provides more narrow size distribution than lower temperature growth[21] because, as explained by Drucker and Chaparro,[21] the energy barrier for edge atom detachment decreases with island size and the faster diffusion kinetics at higher growth temperatures allow these detached edge atoms to more rapidly find the smaller islands producing sharper island size distributions. Here we find that high temperature growth results in undesirable nonuniform composition distribution within QD islands. QD growers need to balance between these positive and negative effects in choosing the growth temperature.

ACKNOWLEDGMENTS

The authors thank the Australian Research Council for providing financial support. This work was also supported by the National Natural Science Foundation of China under Grant No. 69776010.

[1] K. Eberl, Phys. World **10**, 47 (1997).
[2] G. Burkard, D. Loss, and D. P. DiVincenzo, Phys. Rev. B **59**, 2070 (1999).
[3] K. Leonardi, H. Heinke, K. Ohkawa, D. Hommel, H. Selke, F. Gindele, and U. Woggon, Appl. Phys. Lett. **71**, 1510 (1997).
[4] N. Liu, J. Tersoff, O. Baklenov, A. L. Holmes, Jr., and C. K. Shih, Phys. Rev. Lett. **84**, 334 (2000).
[5] T. Wiebach, M. Schmidbauer, M. Hanke, H. Raidt, and R. Köhler, Phys. Rev. B **61**, 5571 (2000).
[6] A. Rosenauer, U. Fischer, D. Gerthsen, and A. Förster, Appl. Phys. Lett. **71**, 3868 (1997).
[7] T. Walther, C. J. Humphreys, and A. G. Cullis, Appl. Phys. Lett. **71**, 809 (1997).
[8] X. Z. Liao, J. Zou, D. J. H. Cockayne, Z. M. Jiang, X. Wang, and R. Leon, Appl. Phys. Lett. **77**, 1304 (2000).
[9] S. A. Chaparro, J. Drucker, Y. Zhang, D. Chandrasekhar, M. R. McCartney, and D. J. Smith, Phys. Rev. Lett. **83**, 1199 (1999).
[10] X. Z. Liao, J. Zou, X. F. Duan, D. J. H. Cockayne, R. Leon, and C. Lobo, Phys. Rev. B **58**, R4235 (1998).
[11] S. Matsumra, M. Toyohara, and Y. Tomokiya, Philos. Mag. **62**, 653 (1990); M. F. Ashby and L. M. Brown, Philos. Mag. **8**, 1083 (1963).
[12] X. Z. Liao, J. Zou, D. J. H. Cockayne, R. Leon, and C. Lobo, Phys. Rev. Lett. **82**, 5148 (1999).
[13] X. Z. Liao, J. Zou, D. J. H. Cockayne, J. Qin, Z. M. Jiang, X. Wang, and R. Leon, Phys. Rev. B **60**, 15605 (1999).
[14] S. A. Chaparro, Y. Zhang, J. Drucker, D. Chandrasekhar, and D. J. Smith, J. Appl. Phys. **87**, 2245 (2000).
[15] http://www.strand.aust.com
[16] C. J. Humphreys, Rep. Prog. Phys. **42**, 1825 (1979).
[17] Image features of Ge(Si)/Si(001) coherent islands are sensitive to the specimen thickness with a thickness period of about 40 nm (corresponding to the effective extinction distance of the [000]* beam at 300 keV). Image features shown in Fig. 1 can only be observed at some specific thicknesses [say, $\sim 40+40N$ (nm) with $N=0,1,2,...$] and image simulations show that the image features remain the same for these specific thicknesses. Details on the relationship between image features and imaging conditions are not within the frame of this article and will be discussed elsewhere. In this article, we select a thickness that gives the double-cross image features matching those shown in Fig. 1.
[18] The composition gradients for the simulations of Figs. 6(a) and 6(b) were chosen arbitrarily because we only present qualitative comparison between the simulated and experimental images.
[19] G. Wöhl, C. Schöllhorn, O. G. Schmidt, K. Brunner, K. Eberl, O. Kienzle, and F. Ernst, Thin Solid Films **321**, 86 (1998).
[20] K. Sakamoto, H. Matsuhata, M. O. Tanner, D. Wang, and K. L. Wang, Thin Solid Films **321**, 55 (1998).
[21] J. Drucker and S. Chaparro, Appl. Phys. Lett. **71**, 614 (1997).